RSC Advances

ROYAL SOCIETY OF CHEMISTRY

www.rsc.org/advances

In situ synthesis of environmentally benign montmorillonite supported composites of Au/Ag nanoparticles and their catalytic activity in the reduction of p-nitrophenol.

Biswajoy Bagchi[1], Pradip Thakur[2], Arpan Kool[2] Sukhen Das[2]*, Papiya Nandy[2]

[1]Fuel Cell and Battery Division, Central Glass and Ceramic Research Institute, CSIR-CGCRI, Kolkata-700032, India.

[2]Physics Department, Jadavpur University, Kolkata-700032.

*Corresponding author's email id: sdasphysics@gmail.com

Abstract: In the present work, composites of montmorillonite clay supported silver and gold nanoparticles were synthesized by in situ chemical reduction method and characterized by X-ray diffraction (XRD), Fourier Transform Infrared Spectroscopy (FTIR), Uv-vis spectroscopy and Transmission Electron Microscopy (TEM). The clay-nanoparticle composites were synthesized at two different temperatures (25°C and 75°C) where nanoparticle size was found to depend on synthesis temperature. The distribution of the catalytic nanoparticles was uniform in the clay matrix with size in the range of 20-45 nm (at 25°C) and 5-15 nm (at 75°C) respectively. Catalytic activity of the clay-nanoparticle composites were monitored by Uv-visible spectroscopy using p-nitrophenol and $NaBH_4$ as model reactants. The best catalytic efficiency was observed in case of silver-clay nanocomposites with a rate constant of 5.6×10^{-3} sec^{-1}.

Keywords: Clay, metal nanoparticles, composites, catalysis

1. Introduction

The interest in noble metal nanoparticles (NPs) have grown tremendously over time due to their remarkable potential in diverse applications such as electronic, chemical, biological, and pharmaceutical fields [1, 2]. These NPs exhibit some unique physico-chemical properties which distinguishes them from their bulk counterpart. However, optimum utilization of such properties requires fine tailoring because they depend on size, shape, morphology, surface charge which in

turn depends on precursor molecules, synthesis route, nature of reducing agent and coating agent used[3, 4].

Out of several synthesis route reported, wet chemical synthesis has been widely used for producing metal NPs because of high chemical purity, homogeneity and yield of products. The process is also very simple and allows for high degree of versatility leading to tunable metal NPs. However, several hazardous organic and inorganic reagents ($NaBH_4$, CTAB etc) are used in the wet synthesis technique which has raised concerns regarding the impact of chemically grown metal NPs on living organisms and the environment. Consequently, new synthetic routes to produce metal NPs by nontoxic and environmentally acceptable way is gaining importance in research [5].

One of the notable applications of noble metal nano clusters is the catalysis of chemical reactions. Due to their small size and high surface to volume ratio, these NPs exhibit unusually high activity in catalysis with respect to the inactive bulk material [6]. This is of great importance because several toxic inorganic/organic chemicals are released in the environment and accelerated removal of such pollutants by nano-catalysis holds promise for a better ecology.

Especially, reduction of p-nitrophenol (4-NP) which is a non biodegradable toxic environmental pollutant has gained considerable concern [7]. The reaction is also favored because the product 4-aminophenol (4-AP) is of commercial importance serving as intermediate in the synthesis of drugs, anti corrosion agent, photographic developer, hair dyes etc. [8].

Catalytic reduction of p-nitrophenol by CTAB stabilized Au nanoparticles were well studied by Fenger et al and reported dependency of catalytic activity on particle size [6]. Similar size dependency was observed by Gangula et al, where they used biogenic gold and silver nanoparticles to reduce 4-NP [5]. Catalytic activity of chitosan stabilized silver nanoparticle was

studied by Murugadoss and Chattopadhyay, where they reported linear dependency of catalytic activity on nanoparticle concentration [9]. Similar studies were carried out on cationic polynorbornene stabilized silver nanoparticles by Baruah et al. [10]. A somewhat different observation was reported by Pozun et al., where they studied the catalytic effect of different dendrimer encapsulated bimetallic nanoparticles including Au/Cu and Au/Pt on nitro-aromatic compound degradation and reported that the activity is depended on binding energy of 4-NP to nanoparticle surface [11]. Thus the catalytic activity of gold and silver nanoparticles depends on different factors like nanoparticle size, concentration, nature of nanoparticles and catalyst support.

Nanoparticles have a strong tendency to aggregate which reduces their catalytic efficiency and lifetime. Given the high reactivity of metal NPs, it is therefore almost customary to use some coating agents to inhibit aggregation of particles. Again as mentioned above, these coating agents generally includes polymers, inorganic molecules that are toxic to environment and may in some cases, may affect the catalytic property of the NPs designed for specific uses [12]. Bearing this in mind, synthesis routes have been developed in which the NPs have been attached or grown on a solid inert support which not only act as a protective matrix but also provides high surface area to the overall composite by dispersing the particles [13]. Corma and Serna studied selective hydrogenation of nitro groups by gold nanoparticles supported on TiO_2 and Fe_2O_3 [14]. Perret et al., reported enhancement of catalytic activity in Mo_2C and Mo_2C/Al_2O_3 supported Au nanoparticles [15].

Additionally, some oxide supports participate in charge transfer reactions with the catalyst further enhancing their activity [16, 17]. Thus the choice of catalyst support is very important for achieving catalytic optimal activity.

In this respect, metal nanoparticle-clay composite systems are a novel breed of composites in the sense that all the characteristics of the nanoparticles are fully retained with added advantage of being nontoxic to the environment due to the eco-friendly clay matrix. The clay matrix not only supports the metal nanoparticle but also protects the particles from oxidation and aggregation increasing stability and lifetime. Clays (especially montmorillonite) have a tendency to absorb a variety of compounds on their surface. Additionally, they can also intercalate large number of organic or inorganic cations. This is because, initially, negatively-charged interlayer sites of clays are balanced by small cations like Na^{+}, Ca^{2+} etc. Over time, the clay may replace any foreign species or molecules in between the stacked silicate layers of the mineral causing expansion and swelling or contraction. This property called cation exchange capacity is the basis for the preparation of clay supported nano-composites [18-22]. Further clays can also act as Bronsted and Lewis acids which in combination with the nanoparticles can serve as bi-functional catalysts [19].

In the present work, a facile synthesis route has been developed for synthesis of montmorillonite based nano-composites of gold and silver and characterized by Uv-Vis spectroscopy, XRD, TEM and FTIR. Stable nano-composites were obtained which showed uniformly distributed nanoparticles. Catalytic activity of the hybrids has also been evaluated by reduction of p-nitrophenol by $NaBH_4$.

2. Result and Discussions

2.1 Uv-Vis spectroscopy

Figure 2 shows the Uv-visible absorption spectra of gold and silver clay nano-composites respectively. Both the nano-composites showed prominent surface plasmon bands indicating that

the metal nanoparticles are effectively dispersed in the clay matrix without aggregation. Depending on the synthesis temperature (25°C and 75°C), nano-composites showed corresponding red shifts in the plasmon band. This relates to the formation of smaller sized particles (for Au75 and Ag75 (fig. 2b and d)) at 75°C and relatively larger sized particles at lower temperature of 25°C (fig. 2a and c).

In the MMT-nanoparticle system, since both the clay particles and nanoparticles have less mobility at a low temperature therefore adsorbed particles may coalesce forming agglomerates after *in situ* reduction process. But at elevated temperature such inter particle interactions are minimized (due to increased kinetic energy of the precursor molecules) giving reduced particle size and uniform distribution in the clay matrix [23].

2.2 X-ray diffraction

Phase characterizations of the nano-composites were carried out by X-ray diffraction technique. Figure 3 shows the XRD pattern of nanoparticle loaded clay composites. Pristine MMT (black) showed characteristic reflections in the range $2\theta = 4$ to 70°.

For nanoparticle loaded MMT, reflections due to clay crystallites are reduced and flattened while prominent reflections of metal nanoparticles appear for characteristic crystal planes (111, 200 and 220). This shows that the clay structure is somewhat disrupted after nanoparticle formation but majority of nanoparticles are primarily on the surface of clay platelets as evident from XRD reflections [19, 24]. It is to be noted that during synthesis, MMT is first treated with hydrazine which is reported to cause disruption and separation of layered structure resulting in MMT platelets. In the present case, in situ formed of nanoparticles are deposited on the clay platelets. It was also observed that the clay structure was retained more in case where the smaller size

particles are formed i.e. for Au75 and Ag75 (fig. 3 blue and magenta). Therefore, the size of the nanoparticles formed may also have effect on the stability of clay structure.

2.3 Transmission Electron Microscopy (TEM)

TEM micrographs of nano-composites are shown in figure 4. The nanoparticles were well dispersed in the clay matrix which indicated minimum inter-particle aggregation. The synthesized nanoparticles in the composite were in the range of 10-15 nm (Au75) (fig. 4b) and 5-7 nm (Ag75) (fig. 4d) at 75^{o}C. The same nano-composites showed larger nanoparticle inclusions for Au25 (25-45 nm) and Ag25 (10-15 nm) at 25°C (fig. 4a and c). Figure 5 shows the corresponding particle size distribution of the nanocomposites.

This also supports the red shift in plasmon resonance bands of nanoparticles synthesized at low temperature in uv-visible spectroscopy. The gold nanoparticles were much larger at both the synthesis temperature (25°C and 75°C) and showed inter particle aggregation tendency while silver nanoparticles were smaller with uniform dispersion in the clay matrix. Both the nanoparticles showed more or less spherical morphologies with some oval shaped particles for gold. Since no coating agent was used during synthesis it is therefore evident that the clay matrix plays a vital role in stabilizing the nanoparticles for a sufficient period of time without affecting characteristic properties of individual nanoparticles.

2.4 FTIR

The FTIR spectra of MMT and nanoparticle-MMT composites are given in figure 6. For all the samples, characteristic bands of MMT were present around 3633 cm^{-1} (O-H stretching), 3452 cm^{-1} (inter-layer O-H stretching, H-bonding), 1641 cm^{-1} (H-O-H bending), 1126 and 1042 cm^{-1} (Si-O stretching), 917 and 799 cm^{-1} (Al-OH stretching), 525 cm^{-1} and 464 cm^{-1} for Si-O bending

mode vibrations (Fig. 6) [20]. This indicates that the overall structure of montmorillonite is retained in the nano-composites.

However, in case of these nanoparticle-MMT composites, the bands are somewhat shifted to higher wavelengths and is attributed to probable van der Waals interaction between the oxygen atoms in MMT and metal nanoparticles (Fig. 6). The appearance of a new band around 1402 cm^{-1} in the composites is due to the conformational changes in the metal nanoparticle linked clay [18, 20, 25, 26]. This band is observed to be more prominent in case of silver nanoparticle-clay composites (Ag25 and Ag75) than gold indicating a more intimate interaction of silver nanoparticles with the clay matrix. This may explain the relatively smaller size and uniform distribution of silver nanoparticles in the clay matrix as observed through TEM (fig. 4). As mentioned in the previous section, absence of any coating agent indicates direct interaction of clay particles with naked metal nanoparticles. In most of earlier reporting of clay nanoparticles composites, interaction is based on hydrogen bonding between functional groups on coated nanoparticles. Thus this type of metal-clay direct interaction is primarily based on van der Waals interaction though further investigation is needed on this subject.

2.5 Catalysis

The catalytic model reaction of p-nitrophenol (4-NP) to p-aminophenol (4-AP) by sodium borohydride with nanoparticles-MMT hybrids were investigated using a standard Uv-Vis setup.

An initially yellow solution of p-nitrophenolate turned gradually colourless in a period of 0-10 minutes upon addition of Au/AgNp-MMT. An absorption band centered at approximately 298 nm evolves in the Uv-Vis spectra and indicates the formation of p-aminophenolate, the intensity of which correlates with the concentration of the p-aminophenolate. Catalytic reaction progressed almost instantaneously with no induction time after the addition of AuNp-MMT and

AgNp-MMT. Generally, in system with unsupported metal nanoparticles a typical induction period of about 60 to 90 seconds is observed depending on the size of the nanoparticles. This induction time is attributed to diffusion processes as reported by Wunder et. al. [27]. However, in the present case, since the metal nanoparticles are stationary on the clay matrix such diffusion process is minimized. As a catalytic blank system for reference purposes we mixed p-nitrophenol with sodium borohydride without the addition of gold or silver clay hybrids. The solution remained unchanged for many weeks.

Figure 7-10, shows the catalytic behavior and reaction kinetics of Au-75, Au-25, Ag-75 and Ag-25 respectively at three different concentrations of catalyst (in terms of volume). With the addition of catalyst, the absorption peak (at 415 nm) corresponding to 4-NP gradually decreased within a short interval of 10 minutes. The peak at around 300 nm emerges showing formation of 4-AP due to reduction of nitro functional group in 4-NP. All the reactions followed first order reaction kinetics. The rate constants (K) of the reactions are represented in Table 3.

As evident, all the nano-composites showed good catalytic activity with optimum at a particular concentration. In case of gold nanoparticle hybrids, Au75 (fig. 7d) showed a maximum K value of 4.597×10^{-3} sec^{-1} for 50 µL whereas, for Au25 a value of 7.2×10^{-4} sec^{-1} was observed (fig. 8d). The observed decrease in K value for Au25 is due the large particle size due to inter-particle aggregation as observed through TEM.

However, highest catalytic activity was observed for Ag25 ($K = 5.6 \times 10^{-3}$ sec^{-1}) at 10 µL (fig. 9d). It has been reported by several authors, that the mechanistic pathway of catalytic reduction of p-nitrophenol involves co-adsorption of the reactant and reducing agent (BH_4^-) on the surface of nanoparticle catalyst and subsequent electron relay from BH_4^- to the reactant mediated by catalyst [5, 24, 28]. Fenger et al., reported a size of 13nm to be ideal for catalytic gold

nanoparticles to adsorb p-nitrophenols [6]. Considering this, Au75 and Ag25 both have particle size in the range of 13nm and hence shows good catalytic activity. However, increasing the concentration (volume) of the catalyst decreased the K value for both the nanohybrids (fig. 7-10). This is probably because of increased amount of clay particles masking the nanoparticles from the reactant.

Earlier report of comparative studies between catalytic AuNp/AgNp showed that AuNp is more active than AgNp as latter is prone to oxidation [5]. But in the present case, the opposite was observed where AgNp-MMT hybrids showed maximum catalytic activity with reaction almost complete in less than 3 minutes. This is due to very small average particle size of AgNps compared to Au and is a direct consequence of initial interaction with the clay matrix. During synthesis, Ag^{+} ions from AgCl can easily enter the clay lamellae by cation exchange where they are reduced by hydrazine leading to very small particle size and increased protection by clay matrix. In case of gold, the reacting species is $AuCl_4^{-}$ which is loosely adsorbed and is therefore reduced before entering the clay matrix which causes agglomeration. This is reflected in large particle size, instant AuNp formation (compared to AgNp) and more importantly low catalytic activity of AuNp-MMT hybrids.

It is well known that clay matrix (especially 2:1 layered clays) is effective in not only providing protection to adsorbed nanoparticles but also creates attachment sites for various molecules [20]. Thus the increased catalytic activity of Ag25 observed may be attributed to a combination of multiple factors like protection of Ag nanoparticles from local oxidizing environment, prevention of inter-particle aggregation due to strong attachment to clay surface (it is to be noted from FTIR spectra that AgNps showed more intimate interaction with the clay matrix than AuNps) and most importantly, the clay matrix may itself may act as attachment site for adsorption of p

nitrophenolate ions and $NaBH_4$ creating environment for formation of localized catalyst-reactant-reducing agent complexes facilitating catalysis (fig. 11).

In fact, it has been proposed by Zhou et al., that the p-nitrophenol intercalates between the siloxane layer of montmorillonite and bonds through the ditrigonal space of the siloxane hexagonal units to the inner OH units [29] and clay minerals, especially sepiolite and montmorillonite, are considered to be excellent supports for catalytic molecules. They can also exhibit Brönsted and Lewis acidities, which can be combined with the redox reactivity of metallic nanoparticles adsorbed on their surfaces to produce bi-functional catalysts [30-32]. These interactions bring p-nitrophenolate in close proximity to the adsorbed nanoparticles creating the desired microenvironment for rapid catalysis.

3. Experimental

3.1 Materials

Montmorillonite clay (MMT) (<1μm) (procured from NanoCor, USA), Hydrogen tetrachloroauric acid($HAuCl_4$) (Merck), Silver nitrate($AgNO_3$) (Sigma-Aldrich), hydrazine hydrate(N_2H_4) (Merck), p-nitrophenol(PNP)(Sigma-Aldrich), Sodium borohydride ($NaBH_4$), (Merck, India). All the chemicals are >99% pure.

3.2 Methods

3.2.1 Synthesis of MMT-hydrazine complex:

400 mg of MMT clay was added to 10 mL of de-ionized water containing 1:1 (v/v) hydrazine hydrate (99-100%). The dispersion was then vigorously stirred overnight at 50^0C. The resulting mixture was centrifuged at 15000 rpm for 10 minutes and then vacuum dried to form MMT-hydrazine complex.

3.2.2 Synthesis of clay nano hybrids:

20 mg of MMT-hydrazine complex was dispersed in 15 mL of de-ionized water for 10 minutes under stirring condition at 75^0C. To this solution 100 µL of $HAuCl_4$ (0.1 mM) was added drop wise. The clear solution instantly turned wine red indicating formation gold nanoparticles.

In case of silver, 100 µL of $AgNO_3$ (0.1mM) was added similarly. This time the solution turned yellow after 5 minutes. The solutions were then centrifuged at 17000 rpm for 15 minutes. The resulting pellets were re-suspended in 1 mL of distilled water. Synthesis was also carried out at 25° C keeping all the parameters same where blue and reddish yellow colored suspensions were observed for gold and silver respectively. A schematic diagram of the synthesis route is given in figure 1. It is to be noted that the reducing agent (hydrazine hydrate) used during nanoparticle reduction produces only N_2 and H_2O as byproduct which are inert [33]. This in conjunction with montmorillonite makes the nanoparticle-clay hybrid system ecologically compatible. Table 1 designates the synthesized nano-composites with compositions.

Table 1: Sample designations with respective compositions.

3.2.3 Instrumentation

Absorption spectra of nano hybrids (Ag25, Ag75, Au25 and Au75) were measured by a UV–vis spectrophotometer (Lambda 25, PerkinElmer, USA), in the wavelength range 250–600 nm. Measured amount of samples were first sonicated (for 5 minutes) in aqueous solution and then the dispersion was analyzed after appropriate dilution.

Powder X-ray diffraction (XRD) patterns of Ag75 and Au75 were recorded using a Bruker AXS (Model D8, WI, USA) setup with CuK_α radiation (1.5409 Å) and scan speed of $5^\circ min^{-1}$ and scanning range from 3 to 70 (2θ). Pristine MMT clay was used as reference.

Fourier transform infrared spectroscopy (FTIR) (FTIR-8400S, Shimadzu) was also performed to determine the phases in the composite. Samples were prepared by KBr disk method [20], in which 0.2 g of KBr (spectroscopy grade) was thoroughly mixed with sample powder (1 wt% of KBr) and then made into disks by uni-axial pressing. Measurements were taken by an FTIR-8400S model (Shimadzu, Tokyo) with scanning range set from 400 to 2000 cm^{-1} under Happ-Genzel configuration.

Morphological characteristics of the hydrogels were observed by transmission electron microscope (TEM) (JSM 2100, JEOL Ltd., Japan). A minute quantity of samples were first suspended in aqueous solution and sonicated for 15 min before observation.

3.2.4 Catalysis

A standard catalytic test was performed with 4-NP as reactant and $NaBH_4$ as reducing agent. Initially, 30 µL of 0.1mM 4-NP was mixed with varying concentrations of clay nano hybrids and 200 µL of 0.02mM $NaBH_4$. Finally, the volume was made up to 3 mL in a quartz cuvette. Reduction of 4-NP was monitored at 400 nm for a period of 10 minutes at 30 seconds interval. The background subtraction was done with de-ionized water as the reference. All the spectra were corrected with the average value around 800 nm due to interferences during the catalytic reaction caused by the evolving gas bubbles (hydrogen release). Table 2 represents the variations in the catalytic mixture for clay nano hybrids.

4 Conclusions

A montmorillonite clay based Au/Ag nanoparticle hybrid system is synthesized by *in situ* reduction process. The hybrids showed excellent stability with uniform nanoparticles distribution in the clay matrix with dimensions in the range of 5-50 nm depending on the synthesis temperature. Good catalytic activity was exhibited by both Au/Ag-clay hybrids but AgNp-clay

hybrids were more active than AuNp. It was also observed that hybrids containing finer sized (~ 5-10 nm) nanoparticles showed best results. Increased activity of Ag-clay nano hybrids may be attributed to the protective role of the clay matrix with the nanoparticles and increased reactant-catalyst interaction on the clay surface.

6 Acknowledgement

We are grateful to Council of Scientific and Industrial Research (CSIR) and Department of Science and Technology (DST), Government of India for financial assistance. The authors are also indebted to Dr. Kausik Dana, CSIR-CGCRI for his helpful discussion on the research work.

References

1. M. C. Daniel and D. Astruc, Chem. Rev. (2004), 104, 293-346.
2. A. Muller and A. K. Cheetham, in The Chemistry of Nanomaterials. Synthesis, Properties and Applications, ed. C. N. R. Rao, Wiley-VCH, Weinheim, 2004.
3. S. Coe, W. K. Woo, M. Bawendi and V. Bulovic, Nature (2002), 420, 800-803.
4. D. Varade and K. Haraguchi, Soft matter, (2012), 8, 3743-3746.
5. A, Gangula, R. Podila, Ramakrishna M, L. Karanam, C. Janardhana and A. M. Rao, Langmuir (2011), 27, 15268-15274.
6. R. Fenger, E. Fertitta, H. Kirmse, A. F. Thu¨nemann and K. Rademann, Phys. Chem. Chem. Phys., (2012), 14, 9343-9349.
7. T. L. Lai, K. F. Yong, J.W. Yu, J.H. Chen, Y.Y., Shu and C.B. Wang, J. Hazard. Mater., (2011), 185, 366-372.
8. P. Deka, R. C. Deka and P. Bharati, New J. Chem., (2014), 38, 1789-1793.
9. A. Murugadoss and A. Chattopadhyay, Nanotechnology, (2008), 19, 15603.

10. B. Baruah, G. J. Gabriel, M. J. Akbashev and M. E. Booher, Langmuir, (2013), 29(13), 4225-4234.
11. Z. D. Pozun, S. E. Rodenbusch, E. Keller, K. Tran, W. Tang, K. J. Stevenson and G. Henkelman, J. Phys Chem. C., (2013), 117, 7598-7604.
12. P. K. Khanna, P. More, J. Jawalkar, Y. Patil and N. K. Rao, J Nanopart Res. (2009), 11, 793-799.
13. C. Xu, X. Lai, G. Zajac and D. W. Goodman, Phys. Rev. B: Condens. Matter Mater. Phys., (1997), 56, 13464-13482.
14. A. Corma and P. Serna, Science (2006), 313, 332.
15. N. Perret, X. Wang, L. Delannoy, C. Potvin, C. Louis and M. A. Keane, J. Catalysis, (2012), 286, 172-183.
16. F. Cárdenas-Lizana, S. Gómez-Quero, N. Perret and M.A. Keane, Gold Bull., (2009), 42, 124.
17. E. Florez, F. Viñes, J.A. Rodriguez and F. Illas, J. Chem. Phys., (2009), 130, 244706.
18. V. Belova, H. Mo¨hwald and D. G. Shchukin, Langmuir, (2008), 24, 9747-9753.
19. L. Zhu, S. Letaief, Y. Liu, F. Gervais and C. Detellier, Appl. Clay Sci., (2009), 43, 439-446.
20. B. Bagchi, S. Kar, S. K. Dey, S. Bhandary, D. Roy, T. K. Mukhopadhyay, S. Das and P. Nandy, Colloid and Surf B: Biointerfaces. (2013), 108, 358-365.
21. J.Y. Kim, K. J. Ihn and J. S. Na, J. Ind. Eng. Chem., (2011), 17, 248-253.
22. G. Nagendrappa, Appl. Clay Sci., (2011), 53, 106-138.
23. L. Ai and J. Jiang, Bio. Technol., (2013), 132, 374-377.

24. M. Venkatesham, D. Ayodhya, A. Madhusudhan, N.V. Babu, G. Veerabhadram, Appl. Nanosci. DOI 10.1007/s13204-012-0180-y

25. R. Das, S.S. Nath and R. Bhattacharjee, J. Fluoresc., (2011), 21, 1165-1170.

26. M. B. Ahmad, K. Shameli, M. Darroudi,W. Md. Zin, W. Yunus and N. A. Ibrahim, Am. J. Appl. Sci., (2009), 6(12), 2030-2035.

27. S. Wunder, F. Polzer, Y. Lu, Y. Mei and M. Ballauff, J. Phys. Chem. C, (2010), 114, 8814-8820.

28. K. Esumi, R. Isono and T. Yoshimura, Langmuir, (2004), 20, 237-243.

29. Q. Zhou, R. L. Frost, H. He and Y. Xi, J. Colloid. Inter. Sci., (2007), 314, 405-414.

30. J. B. d'Espinose de la Caillerie and J. J. Fripiat, Catal. Today, (1992), 14, 125-140.

31. O. S. Ahmed, Langmuir, (2003), 19, 5540-5541.

32. C.H. Zhou, D.S.Tong, M. Bao, Z. X. Du, Z.H. Ge and X. N. Li, Top. Catal., (2006), 39 213-219.

33. M. Groushko, A. Kamyshny, K. Ben-Ami and S. Magdassi, J. Nanopart Res., (2009), 11 713-716.

Figure captions

Figure 1: Schematic diagram for the synthesis of nanoparticle-MMT composites.

Figure 2: Uv-visible absorption spectra of nanoparticle-MMT composites: a) Au75, b) Au25, c) Ag75 and d) Ag25.

Figure 3: X-ray diffraction (XRD) pattern of nanoparticle-MMT composites.

Figure 4: Transmission electron micrographs (TEM) of nanoparticle-MMT composites: a) Au25, b) Au75, c) Ag75 and d) Ag25.

Figure 5: Particle size distribution of nanocomposites a) Au25, b) Au75, c) Ag75 and d) Ag25 determined from statistical analysis of the TEM images.

Figure 6: Fourier transform infrared spectra (FTIR) of nanoparticle-MMT composites.

Figure 7: Catalytic reaction kinetics for Au75 with 20, 50 and 100µL additions. Error bars represent the standard deviation of the experiment conducted in triplicate and were assessed by one way ANOVA using graph pad Instat version 5.0 software.

Figure 8: Catalytic reaction kinetics for Au25 with 20, 50 and 100µL additions. Error bars represent the standard deviation of the experiment conducted in triplicate and were assessed by one way ANOVA using graph pad Instat version 5.0 software.

Figure 9: Catalytic reaction kinetics for Ag75 with 5, 10 and 15µL additions. Error bars represent the standard deviation of the experiment conducted in triplicate and were assessed by one way ANOVA using graph pad Instat version 5.0 software.

Figure 10: Catalytic reaction kinetics for Ag25 with 5, 10 and 15µL additions. Error bars represent the standard deviation of the experiment conducted in triplicate and were assessed by one way ANOVA using graph pad Instat version 5.0 software.

Figure 11: Schematic diagram showing probable mechanistic pathway for the catalytic activity of the nanoparticle-MMT composites.

Tables

Table 1: Sample designation with respective compositions.

Table 2: Batch composition for catalytic reactions.

Table 3 Rate constants values for nanoparticle-MMT composites.

Graphical abstract

Montmorillonite clay supported in situ synthesized metal nanoparticles with catalytic activity was provided.

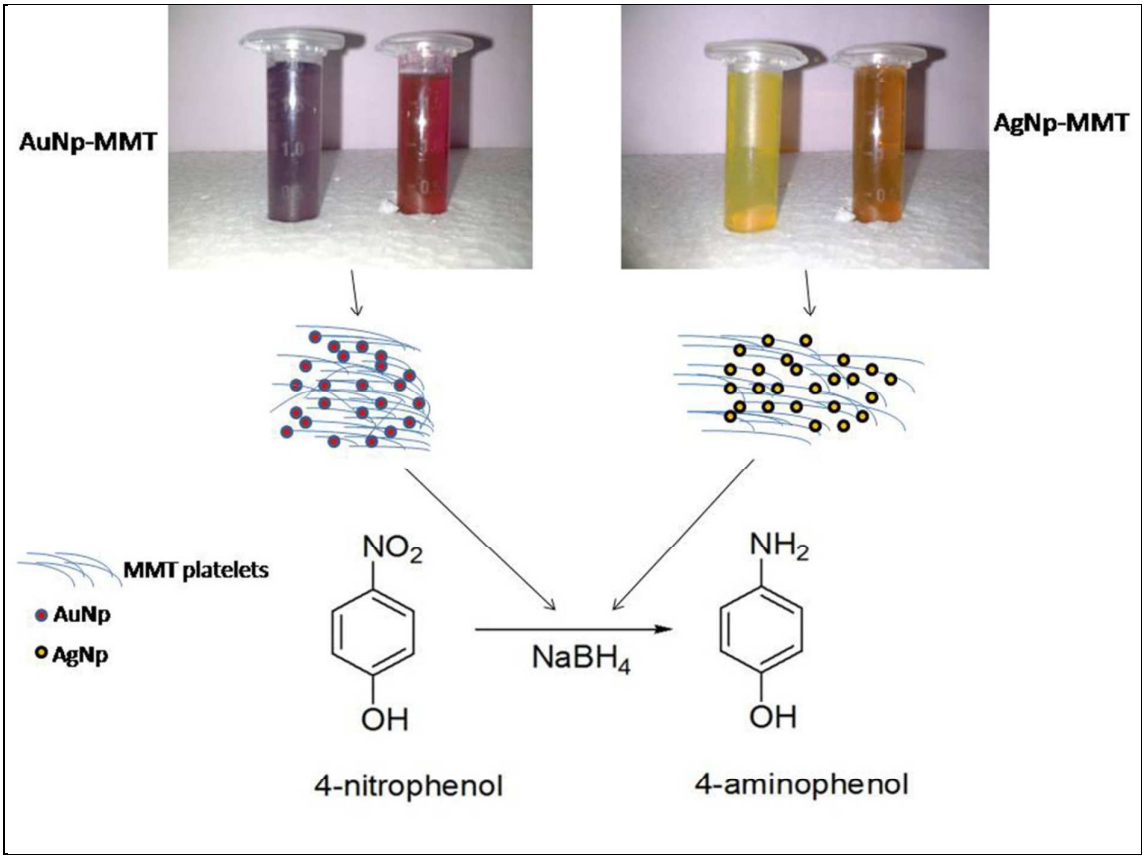

Table 1 Sample designation with respective compositions

Sample	MMT-hydrazine (mg)	Water (mL)	Au/Ag ion conc. (mM)	Synthesis temperature (°C)	Colour
Au25	20	15	7	25	blue
Au75	20	15	7	75	red
Ag25	20	15	0.1	25	reddish yellow
Ag75	20	15	0.1	75	yellow

Table 2 Catalysis reaction compositions

	Au25/Au75 (µL)	Ag25/Ag75 (µL)	PNP (µL)	$NaBH_4$ (µL)	Water (µL)
Set 1	20		30	200	2750
Set2	50		30	200	2720
Set 3	100		30	200	2670
Set 4		5	30	200	2765
Set 5		10	30	200	2760
Set 6		15	30	200	2755

Table 3 Rate constants values for hybrid composites

Sample	volume added (µL)	K (× 10^{-3}) sec^{-1}
Au25	20	0.302
	50	0.72
	100	0.027
Au75	20	0.884
	50	**4.597**
	100	4.298
Ag25	5	5.187
	10	**5.626**
	15	0.701
Ag75	5	5.476
	10	5.067
	15	2.272

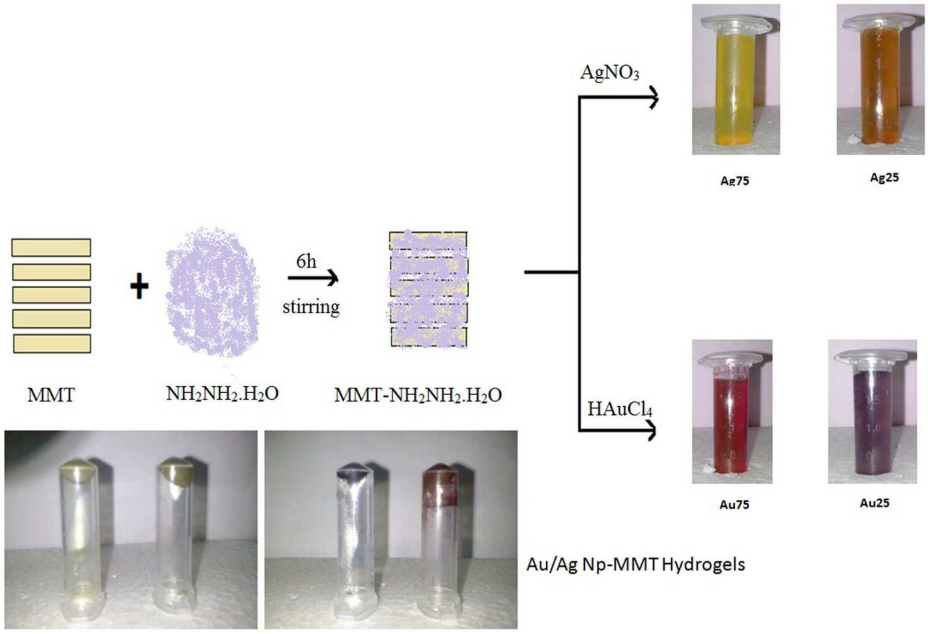

Figure 1
221x158mm (300 x 300 DPI)

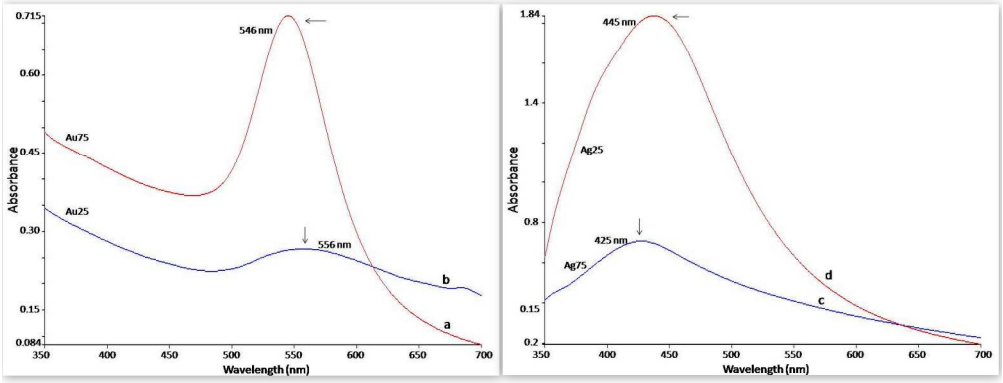

1806x1128mm (100 x 100 DPI)

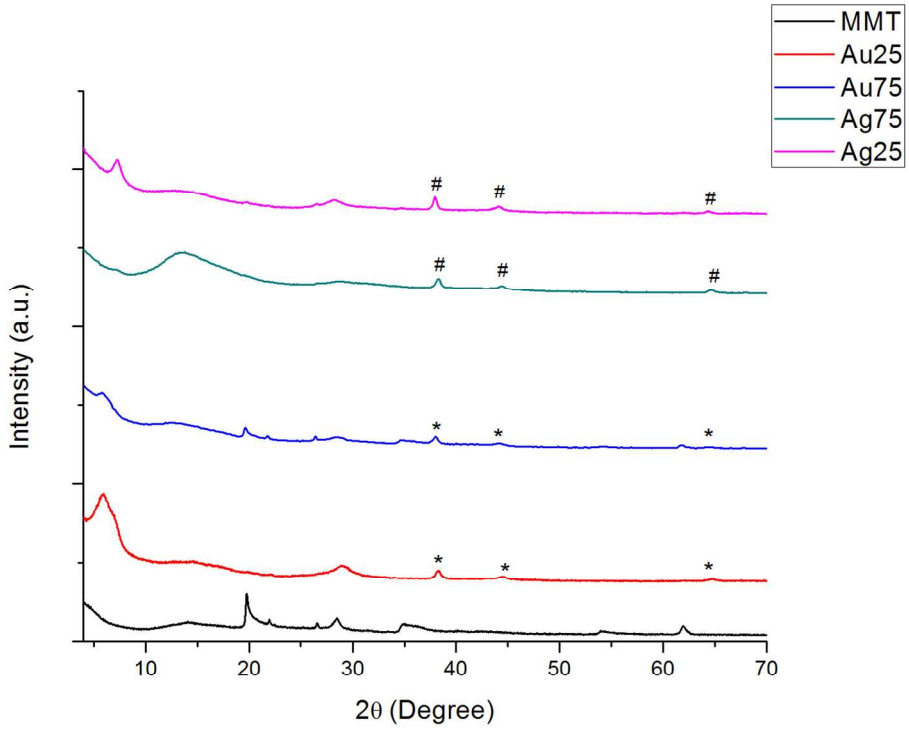

208x160mm (300 x 300 DPI)

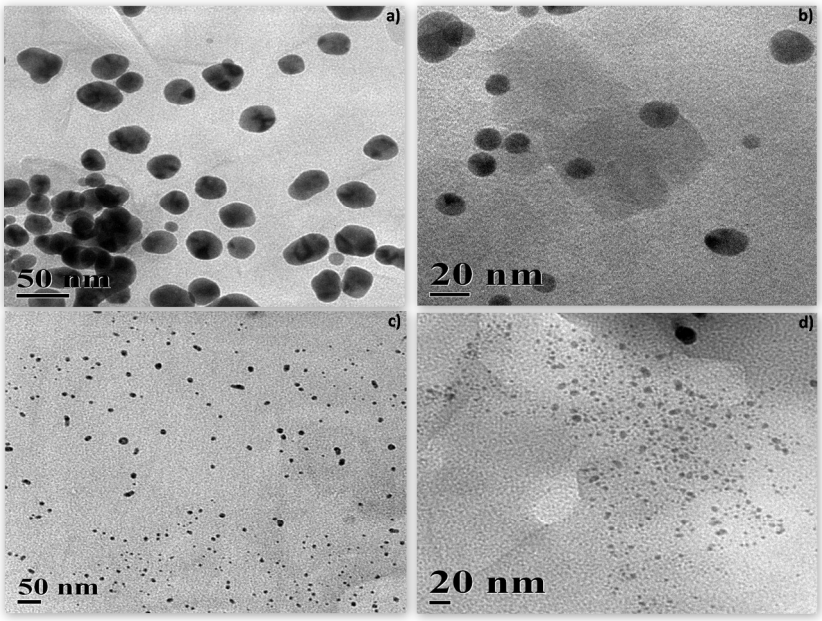

1806x1128mm (72 x 72 DPI)

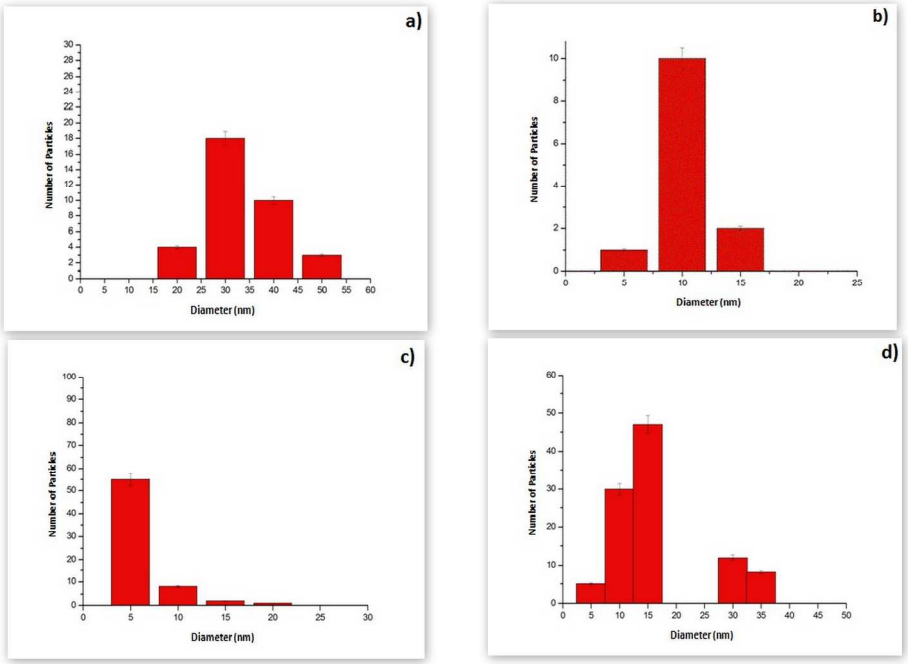

1806x1204mm (72 x 72 DPI)

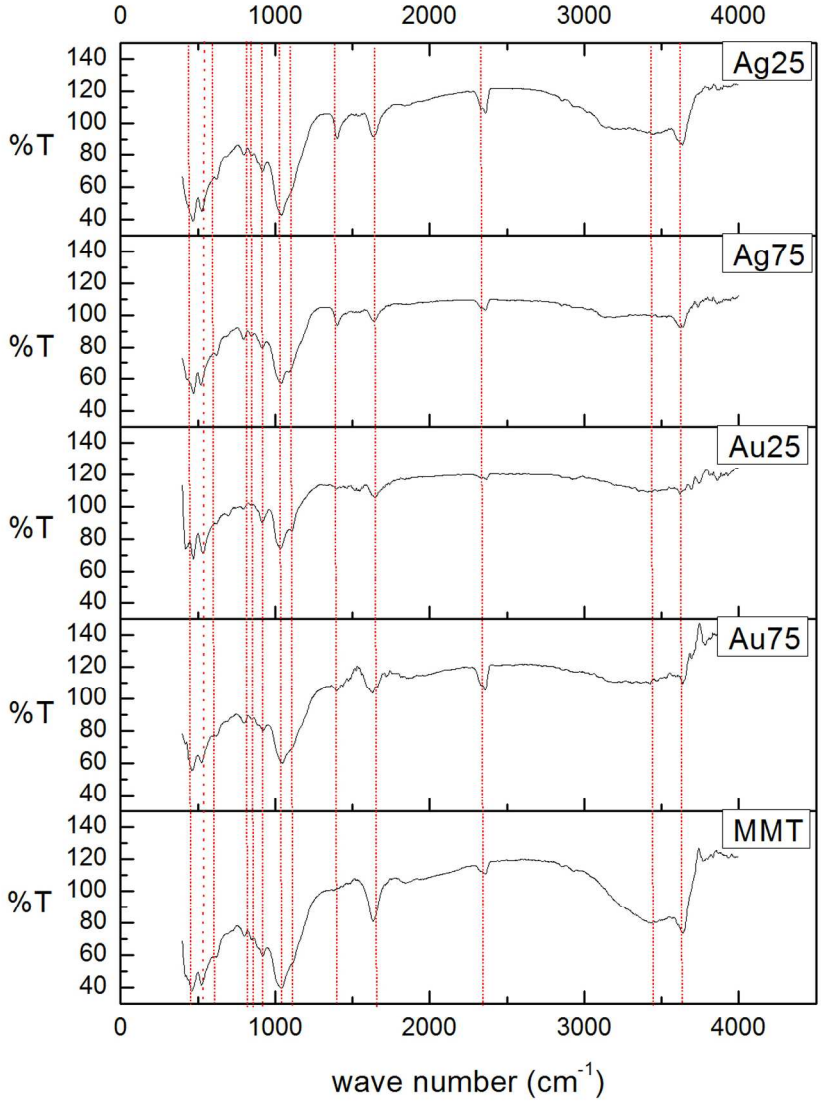

279x361mm (300 x 300 DPI)

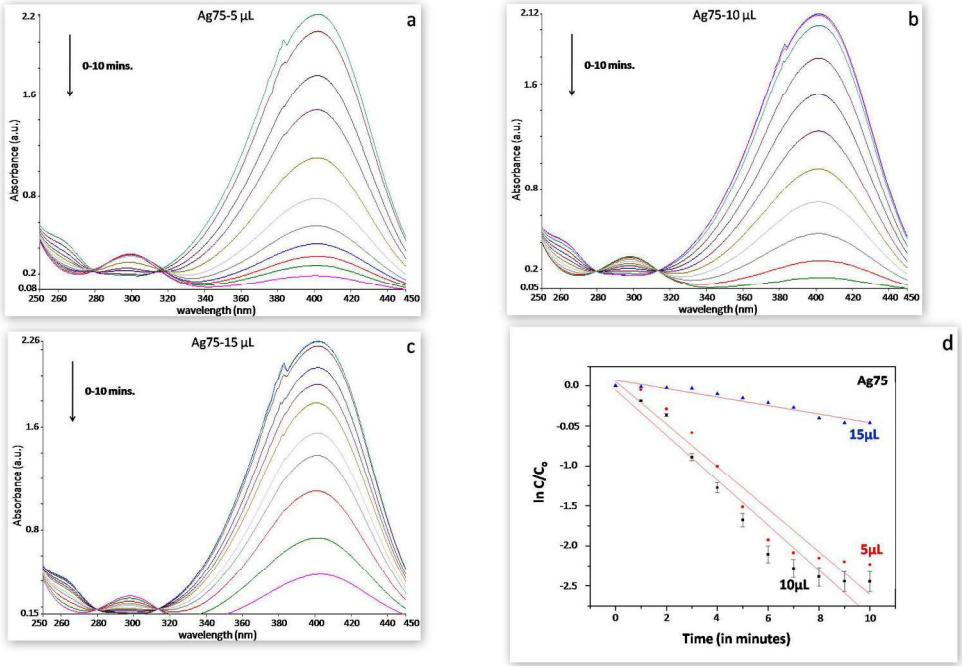

1806x1204mm (72 x 72 DPI)

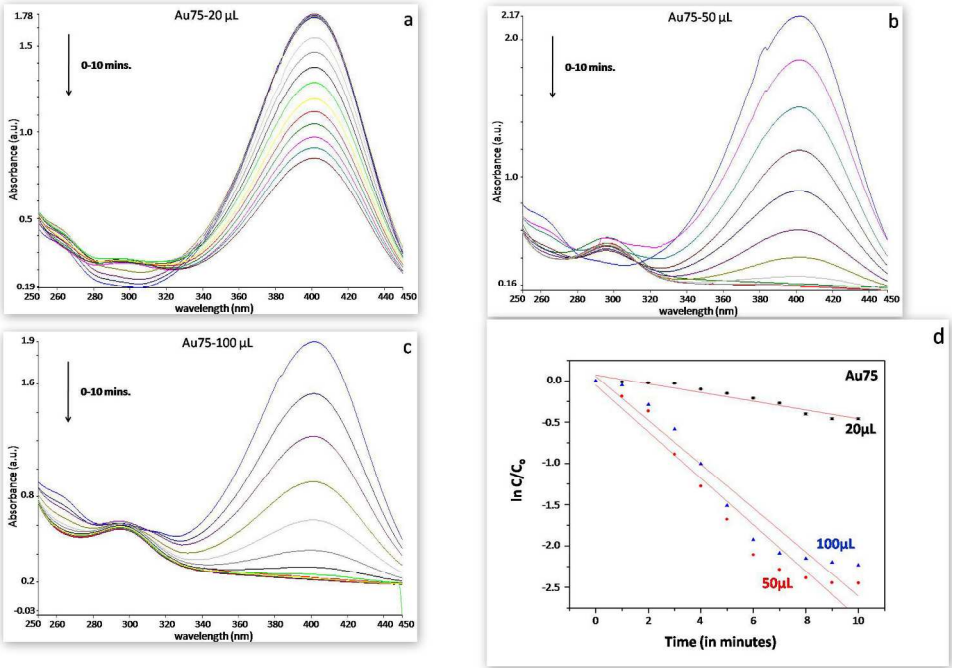

1806x1204mm (72 x 72 DPI)

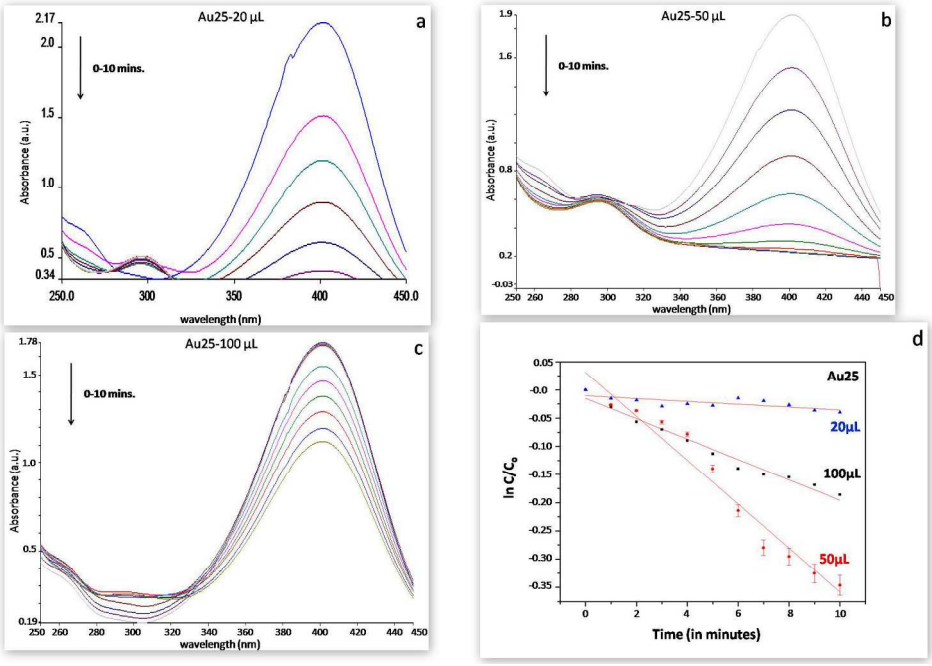

1806x1204mm (72 x 72 DPI)

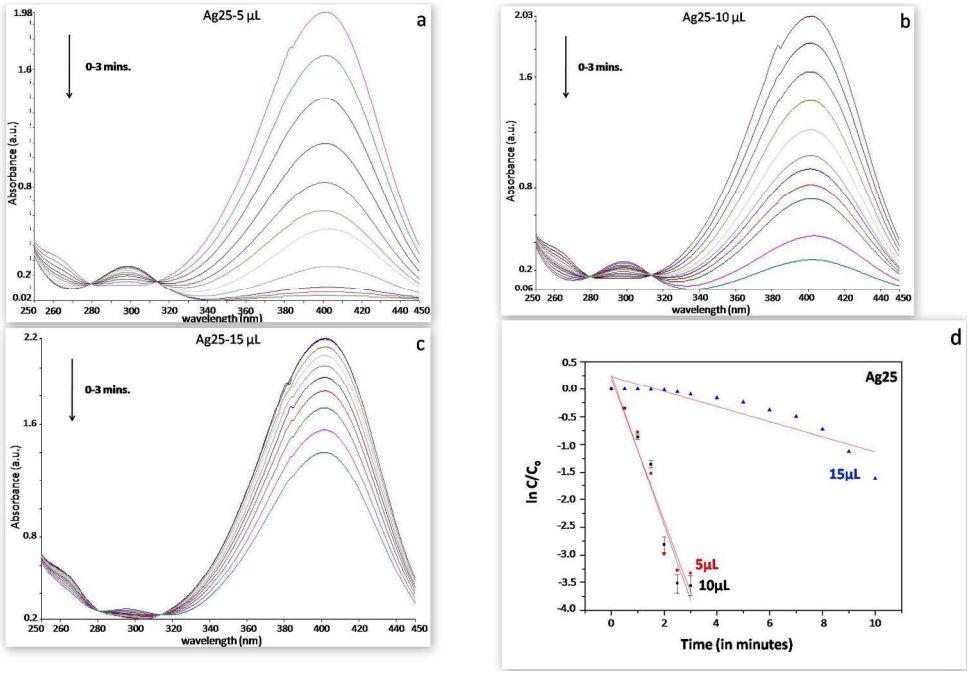

1806x1204mm (72 x 72 DPI)

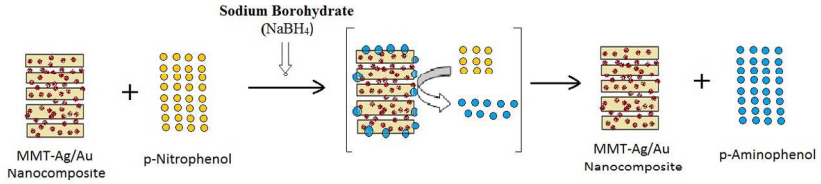

421x200mm (300 x 300 DPI)